Non-contact optical measurement of mechanical gyroscope drift using image processing for spin-stabilized missiles

Pham Khac Lam*, Nguyen Dinh Duy, Le Quang Sy, Duong Dinh Quang

Institute of Missile, Academy of Military Science and Technology, 17 Hoang Sam, Nghia Do, Hanoi, Vietnam.

*Corresponding author: pklambm@gmail.com

Received 16 Jun. 2026; Revised 19 Aug. 2026; Accepted 04 Sep. 2026; Published 16 Sep. 2026.

DOI: https://doi.org/10.54939/1859-1043.j.mst.FMC.2026.201-208

ABSTRACT

This paper presents a non-contact optical system for real-time gyroscope drift measurement under simulated spin-stabilized missile conditions, integrating the laser reflection principle with webcam-based image processing. The gyroscope was mounted on a flange coupled to a servo-motor shaft rotating continuously at 10 Hz to replicate representative missile spin dynamics, with electrical continuity maintained through a multi-channel slip ring. The proposed system demonstrates that gyroscope drift can be reliably measured in a continuously rotating environment using only low-cost, commercially available hardware, providing a practical solution for inertial sensor calibration and performance evaluation in guidance research on spin-stabilized missiles.

Keywords: Gyroscope drift; Image processing; Spin-stabilized missile.

1. INTRODUCTION

In anti-tank guided missiles (ATGMs), particularly those stabilized by rotation about the longitudinal axis, the mechanical inertial gyroscope is a critical component of the on-board guidance system. The device is a three-degree-of-freedom (3-DOF) gyroscope whose gyromotor is mounted in a Cardan gimbal suspension; the outer-gimbal rotation axis is aligned with or coincident with the missile longitudinal axis. Such gyroscopes exhibit readiness times of 0.02 – 0.3 s and a compact form factor compatible with the missile equipment bay. Together with their long operational life and low manufacturing cost, these properties account for their continued use in current systems [1].

The accuracy of a mechanical gyroscope is dominated by drift, which originates from mass unbalance, bearing friction, thermal effects, and parasitic moments along the Cardan gimbal axes [2]. Quantifying mechanical-gyroscope drift on a spin-stabilized missile under flight-representative conditions is therefore a prerequisite for any error-compensation strategy. Several techniques have been reported for this purpose. Earlier approaches employed contact-type angle pick-offs — contact blades and potentiometers fitted to both the inner and outer gimbals — in electromechanical and gas-driven (pneumatic) gyroscopes [3]. Non-contact pick-offs based on Hall-effect sensors have been applied to drift measurement on the ATGM. Spring-driven gyroscopes, by contrast, employ optical non-contact pick-offs (photodiode emitter–detector pairs) to deliver the angular signal to the guidance loop, and their compact form factor precludes accuracy verification by conventional means. Established drift-characterisation methods — precision rate tables, autocollimators, and Allan-variance analysis of the gyroscope electrical output — require expensive instrumentation and are restricted to static or quasi-static base conditions. A non-contact, low-cost, real-time technique capable of quantifying spring-driven-gyroscope drift on a continuously spinning platform is therefore required [4].

This paper proposes a low-cost, non-contact method of sufficient accuracy for measuring the drift of spring-driven gyroscopes used in spin-stabilized missiles. A small planar mirror is bonded to the outer gimbal of the gyroscope, and a collimated laser beam reflected from this mirror is projected onto a diffuse screen. By the optical-lever principle, any angular drift of the outer gimbal

translates into a proportional, geometrically amplified linear displacement of the laser spot on the screen, which is recorded continuously by a USB webcam. The image-processing pipeline — colour segmentation followed by sub-pixel centroid extraction — converts the recorded video into a time series of two-dimensional angular coordinates [5]. To reproduce spin-stabilized flight conditions about the longitudinal axis, the gyroscope assembly is mounted on a rotating platform equipped with a multi-channel slip ring and driven continuously at 10 Hz [6].

2. PROBLEM

2.1. Theoretical foundations

Figure 1 shows schematic diagram of the fixture for measuring drift by the optical method.

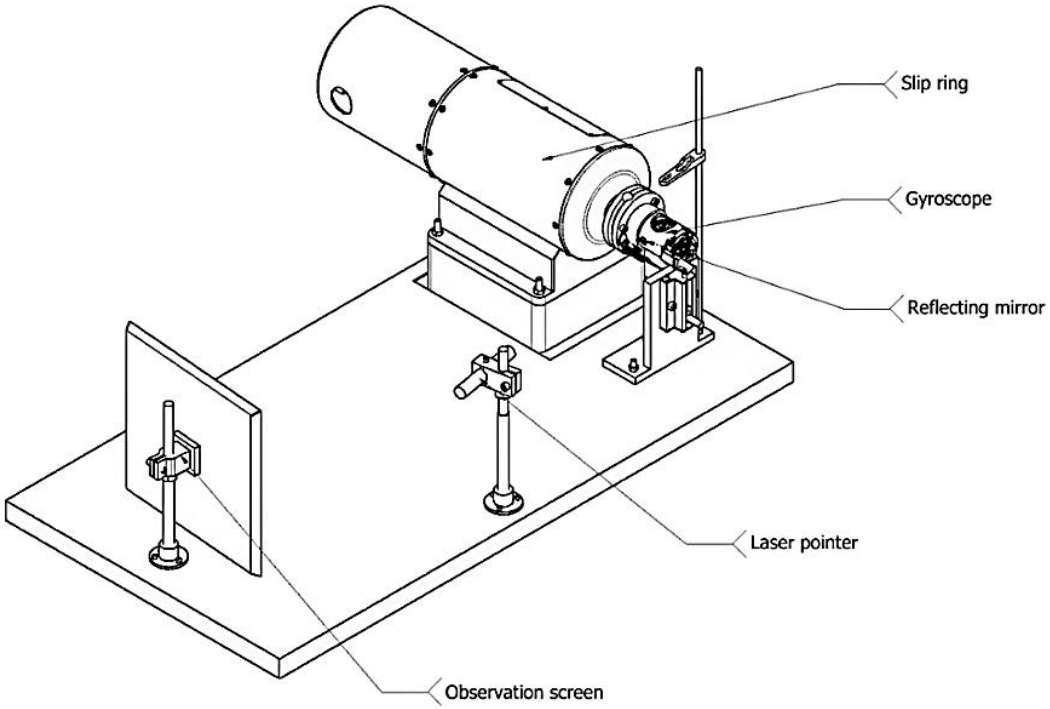


Figure 1. *Schematic diagram of the gyroscope drift measurement setup.*

During the measurement, a planar reflecting mirror is mounted on the outer gimbal of the gyroscope. A laser beam is directed onto the mirror, and the reflected beam is projected onto a receiving screen. The receiving screen is set up so that the incident beam is perpendicular to the screen. At the same time, the laser beam from the laser pointer, the mirror, and the center of the receiving screen all lie in the same plane.

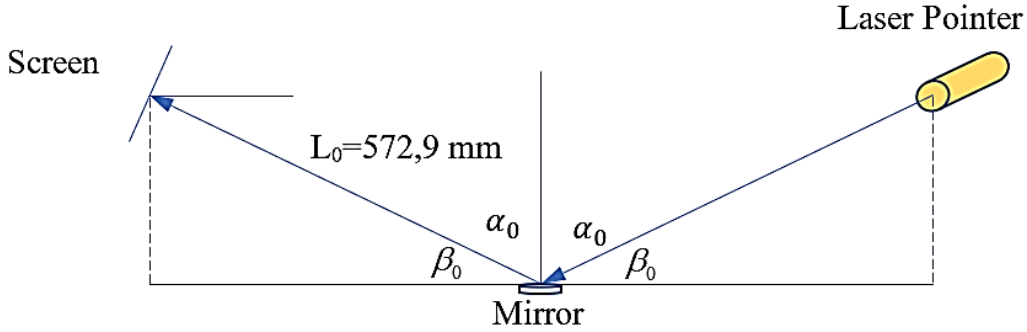


Figure 2. *Optical path of the laser beam from the laser source to the receiving screen.*

As the outer gimbal undergoes angular drift, the mirror rotates accordingly, causing the reflected laser spot to shift across the screen. A webcam is used to capture the laser spot as it moves across the receiving screen. Images are acquired at a sampling rate of 30 Hz, and the centroid coordinates of the laser spot are computed continuously with sub-pixel accuracy. These centroid coordinates are then converted into physical coordinates on the screen plane, from which the drift of the gyroscope is obtained.

In the image plane, the sub-pixel centroid of the segmented laser spot is extracted from its image moments, giving the pixel coordinates (u, v). With the gyroscope mechanically locked, the centroid position (u_o, v_o) is recorded as the working origin.

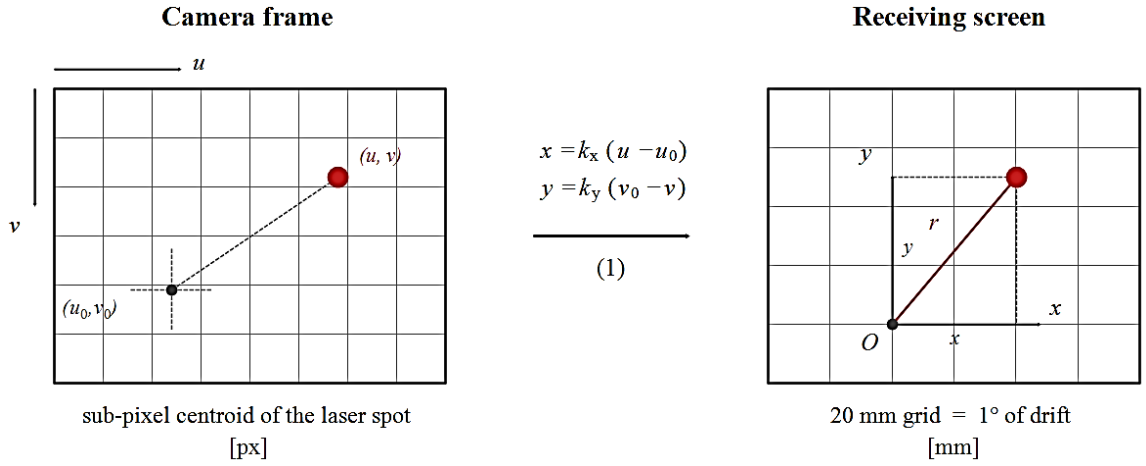


Figure 3. *Measurement of the gyroscope drift by using a webcam.*

The centroid coordinates are converted into physical displacements on the screen plane through the per-axis calibration scales kx and ky, expressed in mm/px:

$$x = k_x (u - u_o)\ ,\ y = k_y (v_o - v) \qquad (1)$$

The sign of the second relation accounts for the downward orientation of the image ordinate. The radial displacement of the spot with respect to the origin is

$$r = \sqrt{x^2 + y^2} \qquad (2)$$

The quantity to be measured is the drift angle of the outer gimbal, denoted α. Since a rotation of the mirror through an angle α deflects the reflected ray through 2α, and the screen stands at a distance L_0 from the mirror, the optical-lever relation $r = L_0 \tan(2\alpha)$ gives the drift angle as

$$\alpha = \frac{1}{2}\arctan\left(\frac{r}{L_0}\right) \qquad (3)$$

The drift of the outer gimbal is determined from the displacement of the laser beam reflected by the mirror mounted on the gyroscope outer gimbal onto the receiving screen. At the initial position, when the gyroscope is mechanically locked, the laser spot is defined as the zero reference.

The specified accuracy requirement for the 9B861 gyroscope is ±5°/20 s. Accordingly, the error in determining the gyroscope drift from the scale divisions on the receiving screen is evaluated. The absolute error between the actual displacement of the laser spot and the corresponding predefined scale division on the screen is given by:

$$\Delta x = (L_0\, tan(2^0) - 20;\ L_0\, tan(4^0) - 40; L_0\, tan(6^0) - 60; L_0\, tan(8^0) - 80\ ;\ L_0\, tan(10^0) - 100) \qquad (4)$$

From there, the absolute error:

$$\Delta x = (-0.96 \cdot 10^{-3} \quad -0.068 \quad -0.225 \quad -0.53 \quad -1.035)$$

Relative error: $\Delta x(\%) = (0.048 \quad 0.17 \quad 0.373 \quad 0.658 \quad 1.035)$

Up to a drift of 5°, the relative error of the linear-grid reading remains below 1.04%. This error is of the same order as the residual centroid-extraction uncertainty and is absorbed into the overall spot-position error budget. The screen can therefore be used as a direct linear scale calibrated in degrees of drift, without any per-angle non-linear correction.

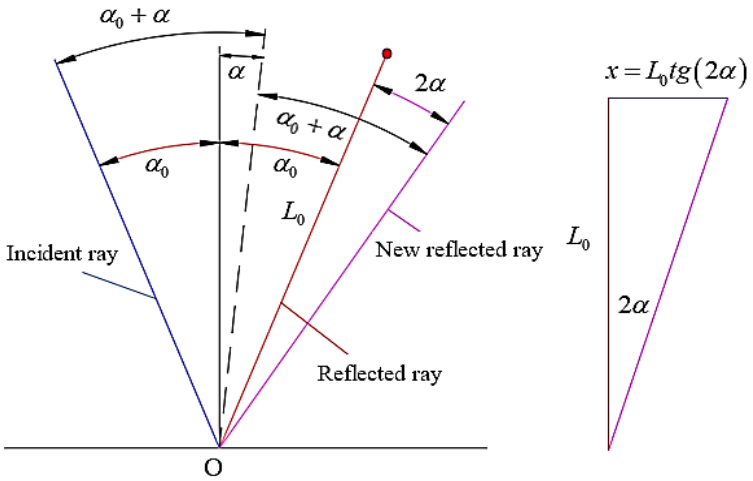


Figure 4. *Optical-lever geometry.*

2.2. Materials and methods

The spring-gyroscope drift measurement system

The spring-gyroscope drift measurement system comprises three main subsystems: a mechanical fixture that reproduces the operating conditions of the gyroscope on a missile spinning about its longitudinal axis; a central control unit that acquires the sensor data and generates the drive pulses for the HBS57 driver; and a custom software application, GyroGUI, that processes the video stream, logs the synchronized data, and provides the operator interface.

The fixture mounts the gyroscope onto a flange coupled to the shaft of a MOFLON MT50119-P0610-S06-VD electrical slip ring. The slip-ring shaft is driven by an HBS57 motor driver paired with a Leadshine 573HBM20-1000 servo motor; the missile spin rate is reproduced at 10 Hz. Electrical continuity during continuous rotation is provided by the slip ring mounted coaxially with the rotation axis.

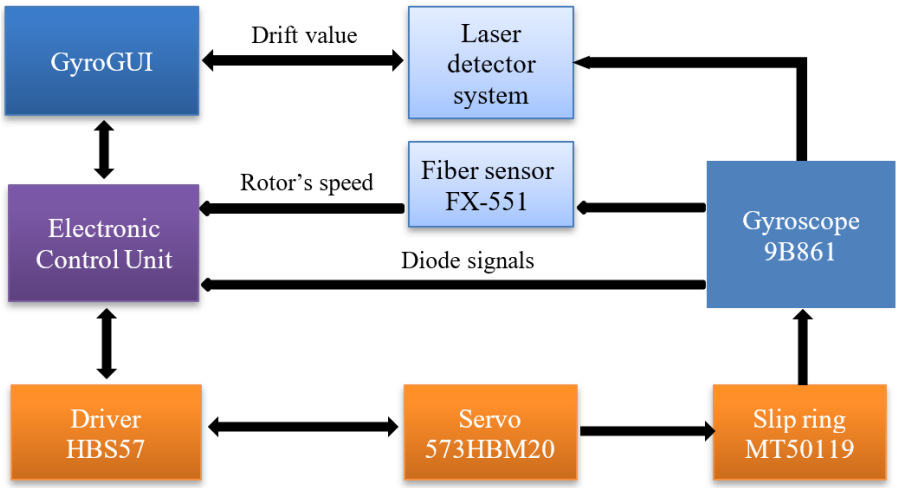


Figure 5. *The spring-driven gyroscope drift measurement system.*

A small planar mirror is bonded to the outer gimbal of the gyroscope, and a collimated red laser ($\lambda \approx 650$ nm) is aligned to strike the mirror at a known incidence angle. The red wavelength is selected for its high webcam sensitivity and high contrast against typical screen materials. The reflected beam falls on a diffuse projection screen placed at distance L from the mirror, and the spot motion is recorded by a USB webcam aimed at the active region of the screen. The fixture, release pin, projection screen, and laser source are rigidly mounted on a single heavy base plate.

For image processing, each captured frame is converted from BGR to HSV; an HSV threshold (H ∈ [0, 40], S ≥ 100, V ≥ 200) isolates the laser colour, with optional inclusion of saturated white regions to recover over-exposed spot cores. Residual noise is suppressed by morphological opening and closing with a 5×5 elliptical kernel. The largest contour with area between 5 and 5 000 px² is retained, and a sub-pixel centroid is extracted from its image moments. The centroid coordinates are converted to physical screen coordinates through the per-axis calibration scales k_x and k_y, and the calibrated origin is subtracted to yield (x, y) relative to the working zero. For visualization and logging, the photodiode signals and the rotor velocity are displayed in real time. The timestamp, commanded rotation rate, encoder frequency, rotation direction, laser-spot coordinates, and derived angular coordinates are recorded to a CSV file for offline analysis.

3. RESULTS AND DISCUSSION

3.1. Input data

A test was conducted on a spring-driven gyroscope mounted on the fixture described in Section 2.2. The recording was started 3 s before the rotor cage release and continued through the rotor run-down phase, giving a total record of $t_f = 25.675$ s. Within this record, three regimes are identified:

Preparation window, $0 \le t < 3.000$ s — the rotor remains caged at $\Omega = 0$ rpm and the gimbal is mechanically locked; the optical pipeline reports the measurement-noise floor of the centroid extractor.

Release transition, $3.000 \le t \le 3.002$ s — the cage is released and the rotor accelerates from 0 to approximately 94% of its peak speed within 2 ms; the encoder-derived speed profile follows the exponential law $\Omega(t) = \Omega_{\max}[1 - \exp(-(t - 3.000)/\tau)]$ with $\tau \approx 0.7$ ms and $\Omega_{\max} \approx 17{,}900$ rpm.

Coast-down, $t > 3.002$ s — the rotor coasts freely under bearing friction and aerodynamic drag, decelerating from $\Omega_{\max} \approx 17{,}900$ rpm at $t \approx 3.002$ s down to $\Omega \approx 10{,}565$ rpm at $t = t_f$.

The complete dataset comprises 10,996 time-stamped samples for each of the channels listed in the CSV file. The rotor-speed trajectory $\Omega(t)$ is shown in Figure 6, and the spin-up transition is detailed in Figure 7.

The 3-s preparation window precedes the cage release at t = 3 s; thereafter the rotor coasts down under bearing friction and aerodynamic drag.

The encoder-derived rotor speed follows an exponential rise with time constant approximately 0.7 ms and reaches 94% of peak within 2 ms of release. The drift angle $\theta_d(t)$ was extracted from the recorded video stream by the image-processing pipeline, HSV colour segmentation isolates the laser spot in each frame; morphological cleaning and largest-contour selection remove residual noise; and a sub-pixel centroid is obtained from the image moments.

The centroid coordinates are then mapped to physical screen coordinates and to gimbal angles through the optical-lever relation of Section 2.1. Time-aligned recording of the rotor speed and the drift angle is provided by the synchronisation reference.

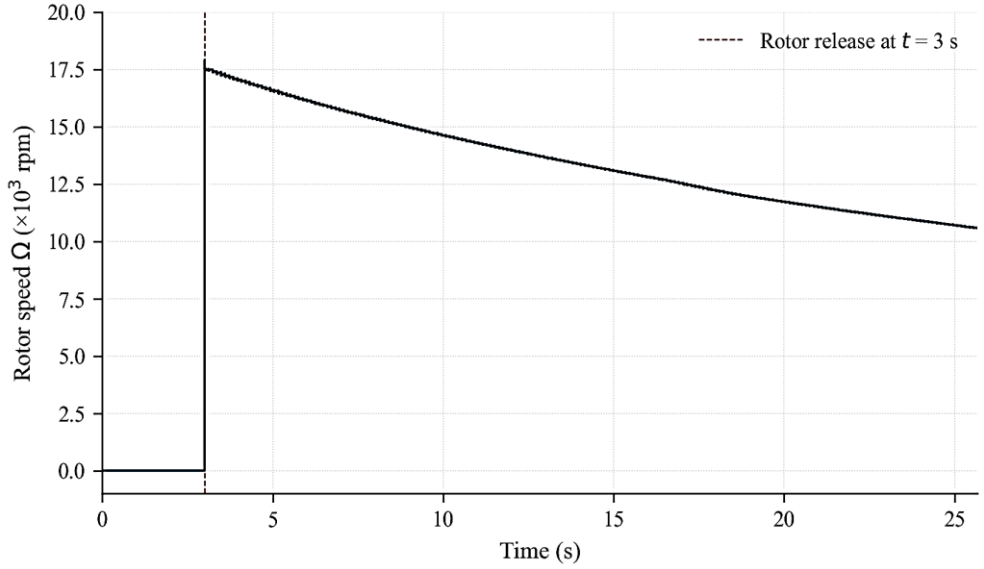


***Figure 6**. Rotor speed $\Omega(t)$ over the full test record.*

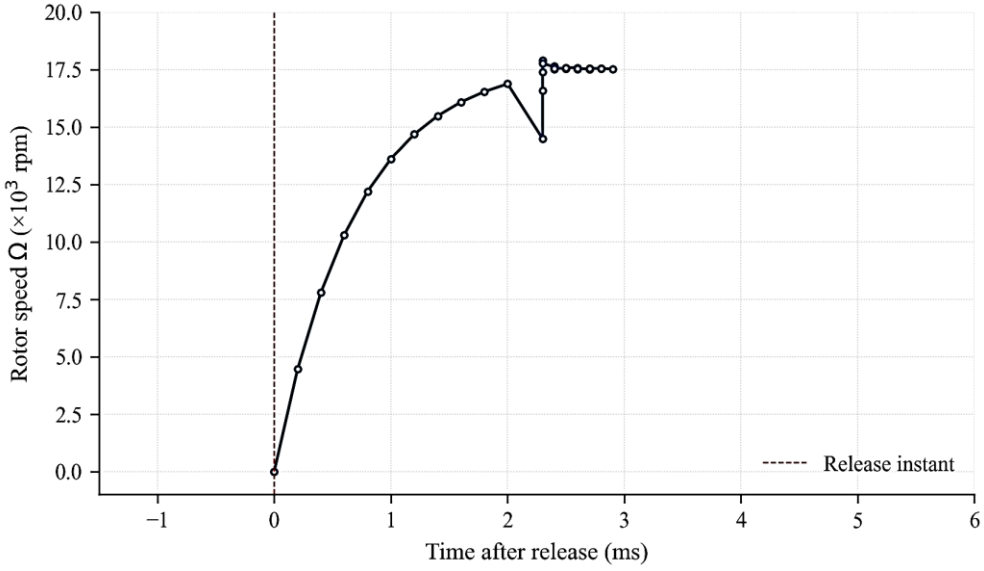


***Figure 7.** Detail of the rotor spin-up transition immediately after release.*

3.2. Results and comments

The recovered drift trajectory $\theta_d(t)$ is shown in Figure 8. During the preparation window, the drift signal fluctuates within $\pm 0.05°$ around zero — the centroid-extraction noise floor for a stationary, caged gimbal. From the rotor release at $t = 3$ s, the drift angle begins to accumulate and develops gradually as the rotor coasts down. By the end of the record, the drift reaches $\theta_d(t_f) = +1.28°$, with a mean of $+0.55°$ and a standard deviation of $0.38°$ over the coast-down window; the peak instantaneous value is $+1.33°$.

Linear-fit drift rates over five contiguous five-second windows are summarised in Table 1. The mean drift rate increases by approximately 27% between the first and the fourth window, while the corresponding rotor speed decreases by 22%. The trend is consistent with the precession relation $\omega_d = M_d/H$ with $H = J_r\Omega_r$: as Ω_r decreases, the same disturbance moment M_d produces a larger drift rate.

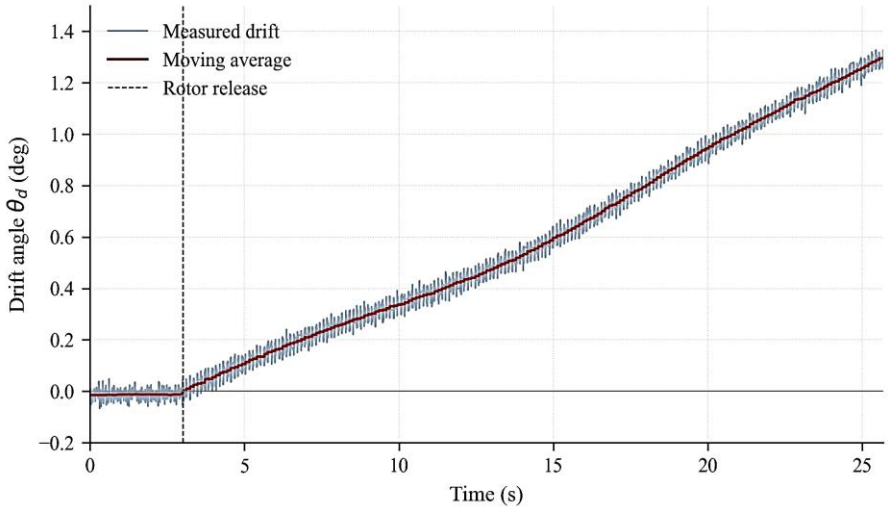


Figure 8. *Recovered drift trajectory$\theta_d(t)$. The thin curve is the raw measurement; the bold curve is a sliding-window mean. The drift remains within the noise floor during the 3-s preparation window and grows monotonically once the rotor is released.*

Table 1. *Mean drift rate and corresponding mean rotor speed in successive five-second windows.*

Window (s)	Mean rotor speed (rpm)	Mean drift rate (°/s)
3–8	14 994	+0.052
8–13	14 641	+0.044
13–18	13 060	+0.063
18–23	11 754	+0.066
23–25.7	10 877	+0.059

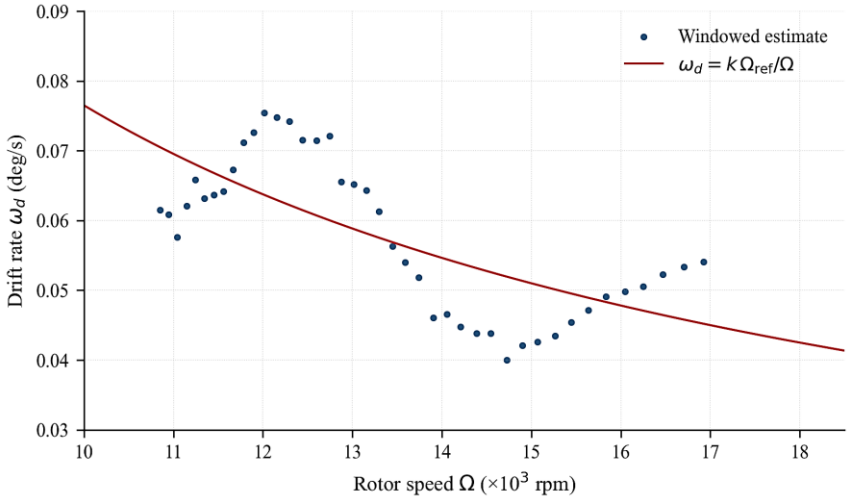


Figure 9. *Drift rate ω_d as a function of rotor speed.*

The drift rate is observed to increase with rotor deceleration, in agreement with $\omega_d \propto 1/\Omega$.

4. CONCLUSIONS

This paper has presented a non-contact optical method for real-time measurement of mechanical gyroscope drift under conditions representative of spin-stabilized missile flight,

addressing the need for accurate drift characterization in the guidance systems of missiles — particularly anti-tank guided missiles (ATGMs) that spin about their longitudinal axis. In contrast to conventional techniques based on precision rate tables and other expensive instrumentation, which require static platform conditions or provide only indirect electrical-domain measurements, the proposed system integrates the laser-reflection (optical-lever) principle with webcam-based image processing. The gyroscope was mounted on a flange coupled to a servo-motor shaft rotating continuously at 10 Hz — with electrical continuity maintained through a multi-channel slip ring — to replicate representative missile spin dynamics. A collimated laser beam reflected from a planar mirror on the outer gimbal was projected onto a screen, where a USB webcam and a centroid-based sub-pixel localization algorithm determined the spot displacement, and hence the gimbal drift, in real time.

The method was demonstrated on a representative test campaign covering 25 s of data — a 3 s preparation window, a sub-millisecond rotor release at t=3 s, and a 22 s coast-down — during which the rotor speed decreased from 17900 to 10565 rpm. The measured drift angle grew monotonically from the noise floor of ±0.05° to +1.28° at the end of the record, with a mean drift rate of 0.055 °/s. These results demonstrate that gyroscope drift can be measured reliably with low-cost commodity hardware in a continuously spinning environment that reproduces the longitudinal-axis rotation of a missile at its operational spin rate, rather than on a static base. The proposed system therefore offers a practical solution for inertial-sensor calibration and performance evaluation in spin-stabilized missile navigation research. Beyond research use, the measured drift provides a quantitative basis for performance assessment and can be adopted as an acceptance-testing criterion in the future production of spring-driven gyroscopes.

REFERENCES

[1]. Nguyen Dinh Duy, Phan The Son, Do Tien Can, Tran Ngoc Thanh, *"Regarding the calculation method for a spring-driven gyroscope in rotating aircraft",* Journal of Military Science and Technology, 106, pp. 163-170, (2025).

[2]. D. S. Pelpora, "*Gyroscopic Systems, Part 2*", Vysshaya Shkola Publishers, pp. 14–24, (1971).

[3]. N. F. Babaeva, "*Calculation and Design of Gyroscopic Device Elements*", Mashinostroenie Publisher, p. 46, (1967).

[4]. N. Lysov et al., "*Applied Theory of Gyroscopes*", South Ural State University (SUSU) Publisher, Chelyabinsk, pp. 10–59, (2009).

[5]. G. Bradski and A. Kaehler, "*Learning OpenCV 3: Computer Vision in C++ with the OpenCV Library*", O'Reilly Media, Sebastopol, CA, pp. 10–100, (2017).

[6]. V. I. Gorin and V. Ya. Raspopov, "*Gyro-coordinators for Roll-Spinning Missiles*", Informtekhnika Publishers, pp. 10–21, (1996).

TÓM TẮT

Hệ thống đo quang học không tiếp xúc cho độ trôi con quay cơ khí trên tên lửa xoay quanh trục dọc bằng phương pháp xử lý ảnh

Bài báo trình bày một hệ thống quang học không tiếp xúc để đo độ trôi của con quay theo thời gian thực trong điều kiện mô phỏng tên lửa xoay quoanh trục dọc, kết hợp nguyên lý phản xạ laser với xử lý ảnh dựa trên webcam. Con quay được lắp trên một bích gắn với trục động cơ servo quay liên tục ở tần số 10 Hz để mô phỏng động học xoay đặc trưng của tên lửa, với kết nối điện được duy trì qua một vành trượt nhiều kênh.Hệ thống đề xuất chứng minh rằng độ trôi của con quay có thể được đo tin cậy trong môi trường quay liên tục chỉ với phần cứng phổ thông giá thành thấp, cung cấp một giải pháp thực tiễn cho hiệu chuẩn cảm biến quán tính và đánh giá hiệu năng trong nghiên cứu dẫn đường tên lửa xoay quoanh trục dọc.

Từ khóa: Độ trôi con quay; Xử lý ảnh; Tên lửa xoay ổn định.